Measurement of soil bulk density and water content with time domain reflectometry: Algorithm implementation and method analysis

Journal of Hydrology 598 (2021) 126389

Contents lists available at ScienceDirect

Journal of Hydrology

journal homepage: www.elsevier.com/locate/jhydrol

Research papers

Measurement of soil bulk density and water content with time domain reflectometry: Algorithm implementation and method analysis

Marco Bittelli [a,*], Fausto Tomei [b], P. Anbazhagan [c], Raghuveer Rao Pallapati [c], Pushkar Mahajan [c], Claudia Meisina [d], Massimiliano Bordoni [d], Roberto Valentino [e]

[a] Department of Agricultural and Food Sciences, University of Bologna, Italy
[b] Regional Agency for Prevention, Environment and Energy of Emilia-Romagna, Italy
[c] Department of Civil Engineering, Indian Institute of Science, Bangaluru, India
[d] Department of Earth and Environmental Sciences, University of Pavia, Italy
[e] Department of Chemistry, Life Sciences and Environmental Sustainability, University of Parma, Italy

ARTICLE INFO

This manuscript was handled by Corrado Corradini, Editor-in-Chief, with the assistance of Carla Saltalippi, Associate Editor

Keywords:
Time domain reflectometry
Estimation of bulk density
Dielectric mixing model
New algorithm

ABSTRACT

Time domain reflectometry can be applied to measure soil bulk density. Monitoring of bulk density over large areas for geo-statistical analysis requires a fast and effective method allowing for acquisition of many data points. Methods are available in the literature to obtain density from TDR. However, algorithms for simultaneous measurements of density and soil water content are not available. Moreover, the methodologies presented in the literature requires tests and evaluation. In this study a new algorithm implemented into a software was developed and the method tested over samples having different textural properties. It is shown that the method provided a measurement of density with an accuracy between 1 and 3 %. The new algorithm implements an automated methodology combined with a non-linear least square optimization, allowing for analysis of many waveforms at a time. Several equations to derive soil water content from electric permittivity were tested, showing that dielectric mixing models provides more accurate results. Moreover, the optimization of parameters allows for analysis and application to multiple materials. The method was confirmed robust and suitable for field-monitoring applications.

1. Introduction

Soil density is an important property affecting relevant processes in hydrology, geotechnical engineering and agricultural sciences. Soil bulk density (SBD) is the ratio of mass of dry soil and volume. SBD affects the relative ratio of the soil phases (solid, liquid and gas), and therefore most of the soil parameters that are important to compute water, heat and gas flow (Bittelli et al., 2015). The hydraulic properties, namely the soil water retention and the hydraulic conductivity curves, are affected by pore size distribution and total porosity. When a soil is compacted, its density increases and pore volume and pore size distribution change depending on its texture and structure. Therefore density has an important effect on hydraulic properties and consequently on soil water transport and soil water balance.

Thermal properties are also affected by density. Thermal conductivity and capacity depend on the conductivities and capacities of the individual soil phases. Therefore, a change in the relative ratio of the phases, determined by a change of density, affects the overall soil thermal properties (Bittelli et al., 2015). When the relative ratio of solid particles and voids is changed, the thermal conductivity changes. Overall, density affects the majority of flow processes and physical properties of soils, and it is present in most of the soil parametric equations to estimate fluxes of matter and energy in porous media.

Standards to measure SBD are defined depending on the field of interest. The Soil Science Society of America (SSSA) provides a detailed description of the most common methods to measure SBD (Grossman and Reinsch, 2002). The standard for measuring SBD in agricultural, hydrological and geo-technical applications is still the classic method, where a known volume of soil is collected (usually a sampler of cylindrical shape), and its weight is measured to obtain the density. If the soil is oven-dried, a dry-density is obtained, called soil bulk density (SBD). Otherwise, if water is not removed, a wet-density is obtained, usually called wet soil bulk density (WSBD).

The American Society for Testing and Materials (ASTM) also provide

* Corresponding author at: Department of Agricultural and Food Sciences, University of Bologna, Italy, Viale Fanin, 44, 40100 Bologna, Italy.
E-mail address: marco.bittelli@unibo.it (M. Bittelli).

https://doi.org/10.1016/j.jhydrol.2021.126389
Received 25 January 2021; Received in revised form 22 April 2021; Accepted 24 April 2021
Available online 29 April 2021

standards for measuring SBD. The most common ASTM methods are: the ring and water replacement method (ASTM, 2013), the rubber balloon method (ASTM, 2015), the sand replacement method (ASTM, 2016) and the drive cylinder method (ASTM, 2017).

In natural conditions and even more in disturbed human settings (such as in agricultural fields) density changes over time and space. However, in most researches, modelling and practical applications often a single value of density is measured at the beginning of the monitoring activity and then the same value is used throughout the monitoring period. In many cases measurements are made in few locations and then applied to an entire field or even a catchment. While scientists are aware of these limitations, measurement of SBD is time consuming and labour intensive, therefore extended measurements of SBD are rarely performed and they are often incomplete. A general review on SBD measurement methods is presented by Al-Shammary et al. (2018).

For this reason, faster and more efficient methods have been object of research for many years. Recently, Time Domain Reflectometry (TDR) was shown capable of simultaneously measure SBD and soil water content (SWC), therefore adding an important method for hydrologists, geotechnical engineers and soil scientists. After papers were published and the method validated (Jung et al., 2013a; Jung et al., 2013b), the methods became an ASTM (2012a) standard. The methodology is presented in details by Jung et al. (2013a) and Jung et al. (2013b) and it will be described in the next sections. The advantage of measuring SBD from TDR is many fold. Portable TDR allows for extended and fast measurements of many points in a field, the procedure can also be automatized when a TDR station is installed, allowing for continuous acquisition of SBD over time.

Originally, the ASTM standard was presented for a specific probe geometry (a closed coaxial probe) limiting the application to laboratory conditions since the closed coaxial is difficult to insert and utilize in the field. Based on these considerations, Curioni et al. (2018) proposed a new formulation that provided reliable results by using commercially available TDR probes with three-prongs, better suited for field monitoring.

For the methodology to be effective, the waveform interpretation must be accurate and fast. Indeed, it is of interest to collect many data points in a field, for instance to perform an analysis of spatial variability of density. Therefore, it is necessary to obtain a method where the user can collect many waveforms with portable TDR and run waveform analysis of hundreds or thousands of waveforms to obtain measurements of SBD and SWC. Moreover, the computer code must allow for modification and optimization of soil parameters. The TDR device collects waveforms of reflected waves. For the analysis to be effective and the results accurate, a key aspect is a correct analysis and interpretation of the waveforms. The algorithm must correctly identify inflection points, first and second numerical derivatives, long time (low frequency) amplitudes and other parameters detailed below.

In the papers presented by Jung et al. (2013a), Jung et al. (2013b) and Curioni et al. (2018), there is no discussion about a methodology or an algorithm for data interpretation and parameters optimization. However, it is mentioned that an algorithm written in R would be available upon request, without further specifications.

While algorithms and software for travel time analysis of TDR waveforms are widely available (see review by Robinson et al. (2003)), an integrated software that simultaneously compute SWC and SBD is not available yet. Moreover, the method of Curioni et al. (2018) requires further testing and corroboration for parameter estimation and testing.

In this paper: (1) a new algorithm and software for TDR-waveform analysis that simultaneously measure SBD and SWC is implemented and tested, (2) the method is tested in an independent laboratory experiment over soils having three different textures and over different values of density and (3) comparison of equations for soil water content measurement is performed. Finally, discussion about potential improvements and limitations of the method is presented.

2. Theory

2.1. Electric permittivity

The relative electric permittivity ϵ_r, is the ratio of the permittivity of the material ϵ (F m^{-1}) and the permittivity of vacuum ϵ_0 (8.85×10^{-12} F m^{-1}):

$$\epsilon_r = \frac{\epsilon}{\epsilon_0} \tag{1}$$

The relative electric permittivity is a complex number, where the real part (ϵ_r') accounts for the energy stored in the dielectric at a given frequency (f) and temperature (T) and the imaginary part (ϵ_r'') describes the electric losses or the energy dissipation. Electric permittivity is a measure of the polarizability of a dielectric material. A dielectric with high permittivity has a higher polarization in response to an applied electric field than a material with low permittivity, therefore it stores more energy in the material.

The complex electric permittivity ϵ^* is written as:

$$\epsilon_r^* = \epsilon_r' - \mathrm{j}\left(\epsilon_{rel}'' + \frac{\sigma_{DC}}{\epsilon_0 \omega}\right) \tag{2}$$

where ϵ_{rel}'' is the imaginary part due to relaxations, σ_{DC} is the electrical conductivity at zero frequency (S m^{-1}), ω is the angular frequency ($2\pi f$) where f is frequency (Hz), and $\mathrm{j}=\sqrt{-1}$ is the imaginary number. Eq. 2 describes the two main processes determining energy losses in wet, porous materials: relaxations and electrical conductivity. Relaxations can be due to ionic polarization, double layer polarization, Maxwell-Wagner effects and the high frequency water dipole relaxations. The second term is due to conduction arising from the material surfaces as a result of electric charges, and from electrolytes in the liquid phase. Relaxations depend on material properties and frequency. In the TDR frequencies, Maxwell-Wagner relaxation is important and it is especially pronounced in soil samples with high surface area such as clay (Robinson et al., 2003).

Olmi and Bittelli (2015) presented an analytical procedure, based on fourth-derivatives, to separate relaxation processes in spectra where multiple relaxations are not clearly identifiable. The method can be successfully employed to fully characterize the dielectric properties of materials with multiple relaxations.

A variety of methods exist in the literature of dielectrics to measure the dielectric permittivity. They can be classified in three classes: (1) Lumped-Impedance, (2) Wave Methods and (3) Quasi-Optical.

(1) Lumped-Impedance are those methods in which the dielectric properties are measured by means of impedance (Z), or admittance (Y), where the sample is placed in a measuring cell and treated as a parallel or series circuit of an ideal (parallel plate or cylindrical) capacitor and an active resistor. These methods are largely used at low frequencies (LF) (10^6-10^7 Hz) and in the radio-frequency (RF) range of the spectrum up to 1 GHz. The electromagnetic (EM) wavelength in these methods is much larger than the sample cell size.

(2) The Wave Methods are the ones in which the dielectric interacts with travelling and standing electromagnetic waves (10^9-10^{11} Hz). In this frequency range, network analysers, as well as waveguide and cavity techniques can be applied in both frequency or time domain. The wavelength in these methods is comparable to the sample cell size. The TDR belongs to the wave methods.

Finally, the (3) Quasi-Optical methods (10^{10}-10^{12} Hz) are the ones in which the wavelengths are much shorter than the sample cell size. In these cases, setups like interferometers or oversized cavity resonators are applied. At sufficiently high frequencies, quasi-optical methods essentially become optical methods.

2.2. Travel time analysis

One of the techniques used by the wave methods is based on the analysis of the travelling time of an electromagnetic wave through a material. The velocity v (m s^{-1}) of an electromagnetic wave is affected by the relative electric permittivity ϵ_r, and the relative magnetic permeability μ_r, as:

$$v = \frac{c}{\sqrt{\mu_r \epsilon_r}} \tag{3}$$

where c is the speed of light, 2.997×10^8 (m s^{-1}). The relative magnetic permeability μ_r is the ratio of the permeability of the material μ and the permeability of vacuum μ_0 (1.25×10^{-6} H m^{-1}):

$$\mu_r = \frac{\mu}{\mu_0} \tag{4}$$

From a mechanical standpoint, the velocity v of an electromagnetic wave travelling through a rod of length d (m), is given by:

$$v = \frac{2d}{t} \tag{5}$$

where t is time (s). For a reflected wave, the number 2 in front of the length is included because the wave is reflected back on the TDR metal rod. For most soils μ_r is equal to 1 (Roth et al., 1990), therefore Eq. 3 can be written as:

$$v = \frac{c}{\sqrt{\epsilon_r}} \tag{6}$$

By equating the definitions of velocity:

$$\frac{c}{\sqrt{\epsilon_r}} = \frac{2d}{t} \tag{7}$$

and solving for ϵ_r:

$$\epsilon_r = \left(\frac{ct}{2d}\right)^2 \tag{8}$$

Eq. 8 allows for obtaining the electric permittivity by measuring the travel time t, since the length of the probe d and the speed of light c are known. When the material is a composite mixture, we refer it as bulk electric permittivity (ϵ_b). Basically, travel time analysis is the analysis of the data represented on the x-axis of the TDR waveform. Fig. 1 shows an example of a TDR waveform and travel time analysis analysed with the software presented in this research.

In the top plate the dotted circles are the TDR measured data. The first red-squared dot from the left (point 1) represents change in impedance (reflection coefficient) where the waveform leaves the cable and enters the probe handle, the second red-squared dot (point 2) represents the change in impedance from the probe handle into the metal rods and the third red-squared dot (point 3) represents the end of the metal rods. The travel time between points 2 and 3 is the one computed to derive the SWC, since the travel time is measured over the metal rods that are inserted into the soil.

The main objective of travel time analysis algorithms is to correctly identify the distance between point 2 and 3. Several algorithms have been presented to compute travel time, and they are described in the review by Robinson et al. (2003). Waveform analysis involves a tangent fitting procedure to determine the second inflection point. The inflection points are identified by using first and second derivative, the tangent lines are computed and their intersections is used to identify the point of the second inflection (bottom plate in Fig. 1).

The algorithm presented in this research is also based on computation of the first, second derivative and tangent lines. However, it also includes a new algorithm for the analysis of the reflection coefficient as described below. The first and second derivative are computed by using a five-points numerical derivative as presented in Burden and Faires (1997).

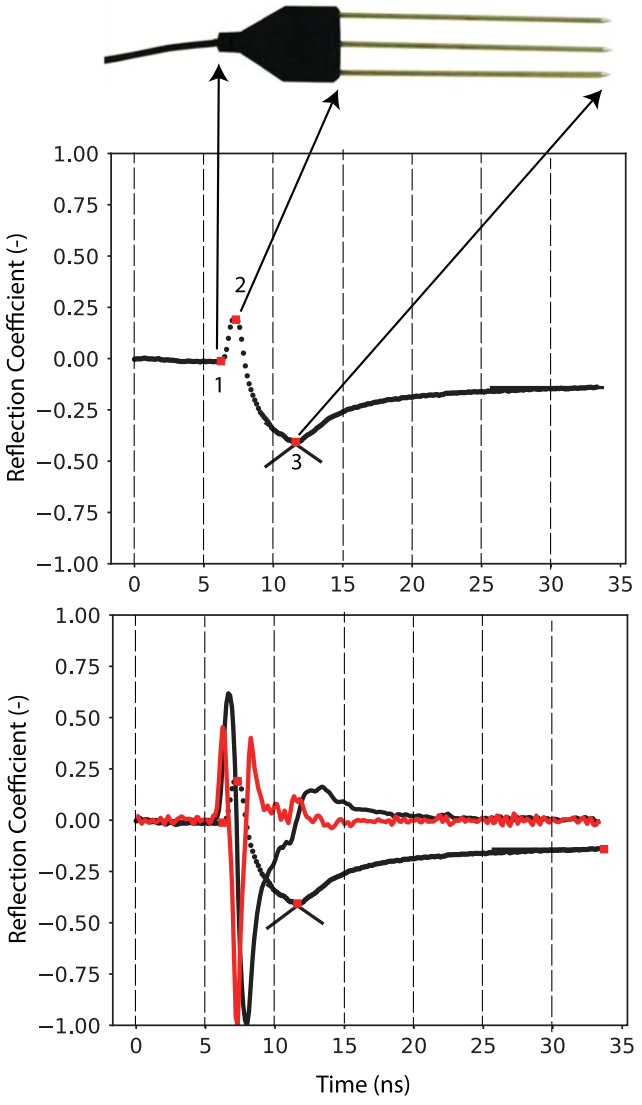

Fig. 1. Example of TDR waveform and TDR probe. The arrows indicate the changes in impedance (reflection coefficient) along the cable, handle and probe. Point 1 indicates the change in impedance from the cable into the probe handle, point 2 the change in impedance from the handle into the metal rods and point 3 the change in impedance at the end of the metal rods, (top plate). Example of TDR waveform (black dots), first derivative (black solid line) and second derivative (red solid line), (bottom plate).

On the waveform curve, the second derivative corresponds to the curvature or concavity of the graph. The graph of a function with a positive second derivative is upwardly concave, in Fig. 1, the first point (point 1) corresponds to the positive maximum of the second derivative. The graph of the waveform with a negative second derivative curve in the opposite way, with the lowest value of the second derivative allowing for identification of point 2. The third value (point 3) is obtained by computing the tangent to the curve by computing the first derivative in proximity of the minimum value, and computing the intersection point of the two tangents as shown in the figure.

After having obtained the travel time, the electric permittivity is obtained by employing Eq. 8. The electric permittivity is used to obtain the SWC as described in the section below about water content measurement.

2.3. Reflection coefficient analysis

Another important information contained in the TDR-waveform is the reflection coefficient, represented on the y-axis of the TDR waveform. The reflection coefficient is given by:

$$\gamma = \frac{V_i - V_0}{V_0 - V_{ref}} \tag{9}$$

where V_i is the measured reflected voltage, V_0 is the voltage in the cable before entering the probe and V_{ref} is the voltage in the cable tester. The attenuation of the energy represented by γ is determined by various phenomena as described above.

The computation of reflection coefficient at shorter times (higher frequencies) has been shown to depend on the material SBD (Jung et al., 2013a; Jung et al., 2013b). Fig. 2 shows (upper plate) the voltage drops used to compute the change in soil compaction as presented by Jung et al. (2013a) and therefore obtain SBD.

The voltage drop between the peak (A) and (B) of the signal is defined as V_1 and called first voltage drop. It is the transient electromagnetic response of the start of the reflected waves from the end of the soil specimen. Points (A) and (B) are the same of points (2) and (3) described above for travel time analysis. The voltage drop V_f is the long-time (low frequency) response when the waveform have stabilised.

The lower plate shows two sand samples measured in this study, for two different levels of compaction and SBD. The two SBD values are indicated by the arrows in the figure. The two values for the point determining V_1 are indicated by (B) and (B1). Clearly the sample at higher SBD determined a higher attenuation of the signal.

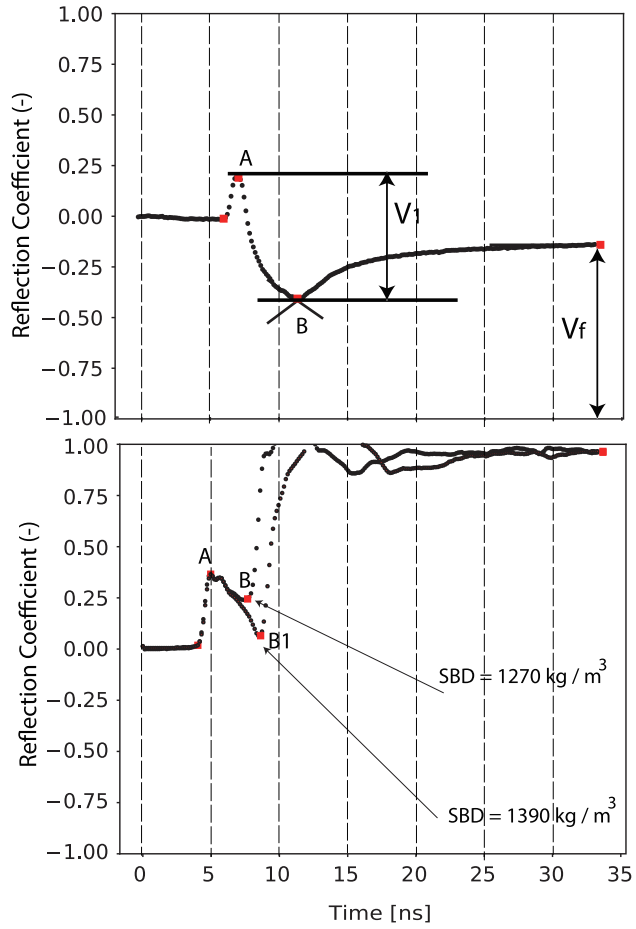

Fig. 2. Example of TDR waveform. Voltage drops along the waveform and changes in reflection coefficient, (top plate). Points A and B are the same as point 2 and 3 in Fig. 1. The values of voltage drop (V_1) and (V_{fw}) are explained in the text. Example of two TDR waveforms having different SBD and SWC (bottom plate). The different values of signal attenuations due to density differences are indicated by the points B and B_1.

The upper trace (the one with point B) had a bulk electric permittivity of 5.8, while the lower curve (the one with point B1) of 10.07. Since the electric permittivity is small it determines the oscillations of the signal at longer times due to the waves travelling faster in materials with low permittivity. The signals at different frequencies no longer travel in phase but they spread out.

Voltage attenuation depends on SBD and therefore its measurement allows for SBD measurement. The algorithm identifies point 2 (here called point A on the y-axis) as described above, the value of the long time values indicated by the red square on the far right is computed by taking the asymptotic last values on the waveform. The magnitude of V_f is computed as the difference between the value at long times and the value of −1 on the y-axis as described in Jung et al. (2013a).

The value of V_f was used in several researches to obtain the bulk direct current (DC) electrical conductivity (Giese and Tiemann, 1975; Heimovaara and de Water, 1993; Castiglione and Shouse, 2015).

At long times (very low frequency approaching zero frequency), the voltage attenuation depends only on the DC conductivity. Giese and Tiemann (1975) presented the following formulation:

$$R_{tot} = \frac{1 + \gamma_\infty}{1 - \gamma_\infty} \tag{10}$$

where R_{tot} is the total DC resistance (Ω), and γ_∞ is the reflection coefficient at infinite time on the waveform, corresponding to the level where the reflection coefficient has reached an asymptotic constant value. Later, Heimovaara and de Water (1993) proposed to separate the resistance into two components:

$$R_{tot} = R_c + R_s \tag{11}$$

where R_c is the cable resistance and R_s is the sample resistance. Castiglione and Shouse (2015) pointed out that this approach was not correct and proposed a more accurate analysis where the reflection coefficient is independent on cable effects and fitting:

$$\gamma_{scaled} = 2\,\frac{\gamma_{sample} - \gamma_{open}}{\gamma_{open} - \gamma_{short}} + 1 \tag{12}$$

where the reflection coefficients γ were computed for open and short circuits. The scaled reflection coefficient (γ_{scaled}) was then used into Eq. 10, in place of γ_∞, to obtain the sample DC resistance. The bulk electrical conductivity, σ_{DC} (S m^{-1}) is the reciprocal of R_{tot}.

The method presented by Jung et al. (2013a) and Curioni et al. (2018) does not explicitly separate the effect of SBD from electrical conductivity. However, it is well known that voltage attenuation depends both on SBD and electrical conductivity (Castiglione and Shouse, 2015). The calibration of the methods of Jung et al. (2013a) and Curioni et al. (2018) with known values of SBD, somehow accounts for this limitation but makes the method highly dependent on parameters as discussed below.

2.4. Soil SBD measurement

Jung et al. (2013a) proposed a relationship obtaining SBD (ρ_d) from measurement of bulk electric permittivity (ϵ_b) and voltage drops.

$$\rho_d = \frac{V_1/V_f}{c_1 + d_1(\epsilon_b - 1) - c_1 \times \exp[(-f_1(\epsilon_b - 1))]}\rho_w \tag{13}$$

where V_1 and V_f are described above, ϵ_b is the measured bulk electric permittivity obtained from travel time analysis, ρ_w is the density of water and c_1, d_1, and f_1 are fitting parameters.

Curioni et al. (2018) pointed out that Eq. 13 was developed for a closed coaxial TDR probe, not suitable for field application. The authors

maintained that if the use of TDR is to be expanded into geotechnical asset monitoring, it would be better if it could be used with off-the-shelf probes that are more suitable for burial, such as the three-rod TDR probes. A new equation for these probes was then proposed:

$$\rho_d = \frac{\rho_w V_r}{a + b\left(V_1\sqrt{\epsilon_b}\right)^c} \tag{14}$$

where $V_r = V_1/V_f$ is the ratio described in Eq. 13, while a, b and c are fitting parameters. The estimation of parameters for 14 will be described in Section 5.

Once the parameters are obtained, SWC (here with symbol θ) can be obtained:

$$\theta = \frac{1}{b} \times \left(\sqrt{\epsilon_b}\ \frac{\rho_w}{\rho_d} - a\right) \tag{15}$$

Since the bulk electric permittivity (ϵ_b) is obtained for the TDR waveform, other equations can also be used to obtain θ. The equations below have also been included in the algorithm presented here.

2.5. Water content measurement

The empirical relationship by Topp et al. (1980) is:

$$\theta = -5.3 \times 10^{-2} + 2.92 \times 10^{-2}\epsilon_b - 5.55 \times 10^{-4}\epsilon_b^2 + 4.3 \times 10^{-6}\epsilon_b^3 \tag{16}$$

where θ is the volumetric water content ($m^3\ m^{-3}$) and ϵ_b is soil bulk electric permittivity. The authors fitted the third order polynomial to TDR data collected in a coaxial transmission line for four soils.

Malicki et al. (1996) includes SBD in the following equation for water content:

$$\theta = \frac{\sqrt{\epsilon_b} - 0.819 - 0.168\rho_d - 0.159\rho_d^2}{7.17 + 1.18\rho_d} \tag{17}$$

where ρ_d is the SBD [g cm^{-3}].

A different approach was proposed by Roth et al. (1990), by using a dielectric mixing model. The dielectric mixing model computes the bulk electric permittivity as a weighted sum of the electric permittivity of each soil constituent:

$$\epsilon_b = \left(\phi_s\epsilon_s^\alpha + \theta\epsilon_l^\alpha + \phi_g\epsilon_g^\alpha\right)^{1/\alpha} \tag{18}$$

where ϕ_s, θ and ϕ_g are the solid, liquid and gas phase volumetric fractions. The corresponding electric permittivities are ϵ_s, ϵ_l and ϵ_g, while α is a geometrical parameter related to the geometrical orientation of soil particles with respect to the electromagnetic field. A default value of 0.5 was used as suggested by the authors. The volumetric solid fraction can be also written as $\phi_s = (1 - \phi_f)$, where ϕ_f is the porosity and the volumetric fraction of the gas phase is $\phi_g = (\phi_f - \theta)$.

$$\theta = \frac{\epsilon_b^\alpha - \left[\left(1 - \phi_f\right)\epsilon_s^\alpha + \phi_f\epsilon_g^\alpha\right]}{\epsilon_l^\alpha - \epsilon_g^\alpha} \tag{19}$$

The dielectric mixing model of Eq. 19 can be written as function of SBD and of the square root of the bulk electric permittivity:

$$\theta = \frac{\sqrt{\epsilon_b} - \left(\frac{\rho_d}{\rho_s}\sqrt{\epsilon_s}\right) - \left(1 - \frac{\rho_d}{\rho_s}\right)\sqrt{\epsilon_g}}{\sqrt{\epsilon_l} - \sqrt{\epsilon_g}} \tag{20}$$

To employ the dielectric mixing model, knowledge of SBD and electric permittivity of the solid phase is needed, as well as the electric permittivity of the liquid phase. In this study the following values were used $\epsilon_g = 1.005$, $\epsilon_l = 80.3$, $\epsilon_s = 4$, $\alpha = 0.5$ and porosity was obtained from the TDR-estimated value of SBD. Since Eq. 14 does not require previous knowledge of soil water content to compute density, but only knowledge of bulk electric permittivity, voltage attenuation and water density, the algorithm first computes bulk electric permittivity (through travel time) and voltage attenuation. Then the value of density is obtained and can be used, in the dielectric mixing model, to compute SWC.

3. Material and methods

To test the algorithm and calibrate the model of Eq. 14, independent measurements of SBD and SWC at different levels of compaction were performed as described below.

3.1. Soils

Three different soil types were used: sand, kaolin clay and silty sand. All the materials were tested in the Laboratory of Geotechnics and Applied Geology of the Department of Earth and Environmental Sciences, University of Pavia, Italy.

The sand was extracted from quarries near the Ticino River owned by the Company "Sabbie Sataf Srl" and it belongs to the so-called "Ticino sand". The factory names the material "116/S-25". According to the Unified Soil Classification System (USCS) it corresponds to a selected sand, with grain size from 0.8 mm to 1.2 mm of diameter.

The kaolin clay belongs to Kaolin powder AkPrime CAPKN80SA sold by the Company "BAL-CO spa" of Sassuolo (Modena, Italy). This material is formed almost entirely by clay particles with diameter lower than 2 μm. Particles with diameter higher than 45 μm are present in negligible quantity of less than 0.3 %. According to the USCS Classification this material is classified as a clay.

The silty sand is formed by 82.8 % of sand, with particles diameter between 0.125 mm and 0.075 mm, and 17.2 % of silt, with particles diameter between 0.075 mm and 0.002 mm. These values were obtained with particle size analysis ASTM (1963) of the material carried out on according to the standard. According to USCS Classification, it is classified as a silty sand.

As discussed above, voltage attenuation of the TDR waveforms depend both on SBD and electrical conductivity. To remove the effect of electrical conductivity on voltage attenuation and therefore obtain a more accurate test of the methodology, the samples were prewashed several times with distilled water, to remove the ions. When the saturated extract displayed low values of electrical conductivity ($\lesssim$2 mS m^{-1}), the samples were then subject to compaction and preparation. Temperature was controlled for all the experiments performed in this study. Six samples were analyzed for sand, eight for silty sand and sixteen for kaolin. The different number was due to the fact that it was increasingly easy to compact material with finer texture.

3.2. Preparation of prescribed SWC and SBD in the molds

Soil samples were prepared at the target SBD by the following three operations: (1) measuring the initial water content of the material; (2) adding distilled water to the samples to obtain an approximate initial water content and (3) compacting the samples till obtaining a desired SBD.

1. The first operation consisted in measuring the initial water content of the material. The samples were pre-washed for ions removal. After that, the samples were weighted and oven-dried at 110° for 24 h to obtain the initial water content.
2. The second operation concerned the addition of distilled water to the samples to reach target values of water content. Distilled water was added at prescribed values to reach a target water content. The values are listed in Tables 1–3 for the three samples. However, the exact target value was an initial approximation, since when a sample is compacted the sample volume reduces and the volumetric SWC changes. The weight basis water content remains unchanged but volumetric water content increases significantly. For this reason the comparison was performed after compaction. The gravimetric values

Table 1
Measured bulk density and SWC for the sand samples. Gravimetric (grav.) and volumetric (vol.) are listed separately.

Sand samples	grav. SWC (%)	vol. SWC (m m^{-3})	SBD (kg m^{-3})
s1-2	0.051	0.065	1275.5
s2-2	0.054	0.077	1438.8
s2-3	0.053	0.074	1398.0
s3-1	0.051	0.071	1387.8
s3-2	0.053	0.076	1438.8
s3-3	0.039	0.059	1530.6

Table 2
Measured bulk density and SWC for the silty sand samples. Gravimetric (grav.) and volumetric (vol.) are listed separately and SBD in two different units.

Silty sand samples	grav. SWC (%)	vol. SWC (m m^{-3})	SBD (kg m^{-3})
m1-1	0.046	0.060	1306.1
m1-2	0.055	0.075	1369.4
m1-3	0.055	0.078	1408.8
m2-1	0.103	0.156	1511.2
m2-2	0.099	0.145	1469.4
m2-3	0.101	0.147	1467.3
m3-1	0.155	0.224	1447.4
m3-2	0.137	0.211	1540.8

Table 3
Measured bulk density and SWC for the kaolin samples. Gravimetric (grav.) and volumetric (vol.) are listed separately.

Kaolin samples	grav. SWC (%)	vol. SWC (m m^{-3})	SBD (kg m^{-3})
k1-1	0.062	0.074	1206.1
k1-2	0.004	0.005	1244.9
k2-1	0.020	0.027	1385.7
k2-2	0.025	0.033	1326.5
k3-1	0.035	0.046	1336.7
k3-2	0.044	0.057	1316.3
k3-3	0.038	0.048	1255.1
k5-1	0.173	0.194	1122.4
k6-1	0.183	0.186	1020.4
k6-2	0.175	0.216	1234.7
k7-1	0.207	0.228	1102.0
k7-2	0.207	0.240	1163.3
k7-3	0.217	0.261	1204.1
k8-1	0.244	0.334	1167.3
k8-2	0.238	0.313	1164.0
k9-1	0.307	0.402	1104.6

were multiplied by the measured target density to obtain the final, independent volumetric value and then the values were compared.

3. The third and last operation regarded the compaction of the soil sample to reach a determined SBD. The material was put into a metal mould and loads were used to compact the material. The samples were prepared by following the ASTM (2012b) standard for laboratory compaction (Fig. 3). No leakage of water was observed or recorded during hammering.

A fixed amount of water was added to a specific mass of soil, and mixed to obtain uniform distribution of water as described above. The samples is then placed into a metal mould (15.1 cm of diameter and 12 cm of height) and compacted in three layers. The number of blows depended on the desired SBD for the sample. TDR measurement was performed, the samples were placed on a scale for weight measurement, and then placed into the oven for wet and dry measurement. As described above, even if the sample is prepared with the same initial water content before compaction, the volumetric water content increases after compaction, therefore the initial water content was never the same as the measured water content after compaction. The gravimetric measurement was converted to volumetric measurement by using:

$$\theta = w \times \frac{\rho_d}{\rho_l} \tag{21}$$

where θ (m^3 m^{-3}) is the volumetric water content, w is the gravimetric water content (kg kg^{-1}), ρ_d (kg m^{-3}) is the SBD and ρ_l is the liquid water density, 998 (kg m^{-3}), at laboratory temperature (20°).

3.3. TDR measurement

For this study, a TDR CS610 (Campbell Scientific Inc., 2015) probe was used (Fig. 3). The original probe length (0.3 m) was reduced to a length of 0.1 m to fit into the metal mold and preserve enough distance from the sides of the metal mold to avoid interactions between the EM wave and the metal mold. Moreover, Ferre' et al. (1998) showed that the sampling volume of three-rod probes is contained in large part within the space between the inner and outer conductors. Curioni et al. (2018) reported that the reading did not change with or without the metallic mould being present (Page 4), confirming the results of Ferre' et al. (1998).

Waveforms were collected by using a Time Domain Reflectometer (Campbell Scientific Inc., 2000) connected to a data CR10X datalogger, Campbell Scientific Inc. (1986) and powered by a rechargeable battery. The experiment was performed with a single probe on individual samples, without the use of multiplexers, to avoid additional dissipations due to multiplexing as discussed in Curioni et al. (2018).

4. Software

TDR-waveform analysis implies a series of operations including data input, data testing, parameter input, travel time and reflection coefficient analysis, parameter optimization, data output and visualization. The original software for TDR-waveform analysis was presented by Bittelli et al. (2015), where the program performed travel time analysis for a single waveform at a time. In this software many new features were added. In particular the software allows for selecting a folder where a number of waveforms are stored and automatically perform travel time analysis and voltage attenuation analysis for each waveform. Thousands of waveforms can therefore be automatically analysed.

After while the algorithm performs a non-linear fitting using the Marquardt (1963) algorithm to obtain the parameters for computation of SBD. The algorithm aims at minimizing the sum of squared residuals for a non-linear equation, by optimizing the parameters space. Specifically, the parameters a, b and c in Eq. 14 are estimated. An output file (`.csv`) is then saved in the same folder, containing the bulk electric permittivity, the voltages (V_1, V_f and V_r), the estimated SBD, the estimated SWC and the fitted parameters.

The algorithm and software presented here is written in Python 3.2 and it is called `TDRPy`. The code is implemented into six files:

1. main
2. readDataFile
3. functions
4. Marquardt
5. travelTime
6. plot

The file `main` defines the global variables, import the experimental data and creates the user interface as shown in Fig. 4. From the `main`, the functions to compute the travel time (`travelTime`) and to SBD (`functions`) are called. The Marquardt optimization algorithm, contained in the file `Marquardt` is also called from the `main`. The interface is created with the Python module `Tkinter`.

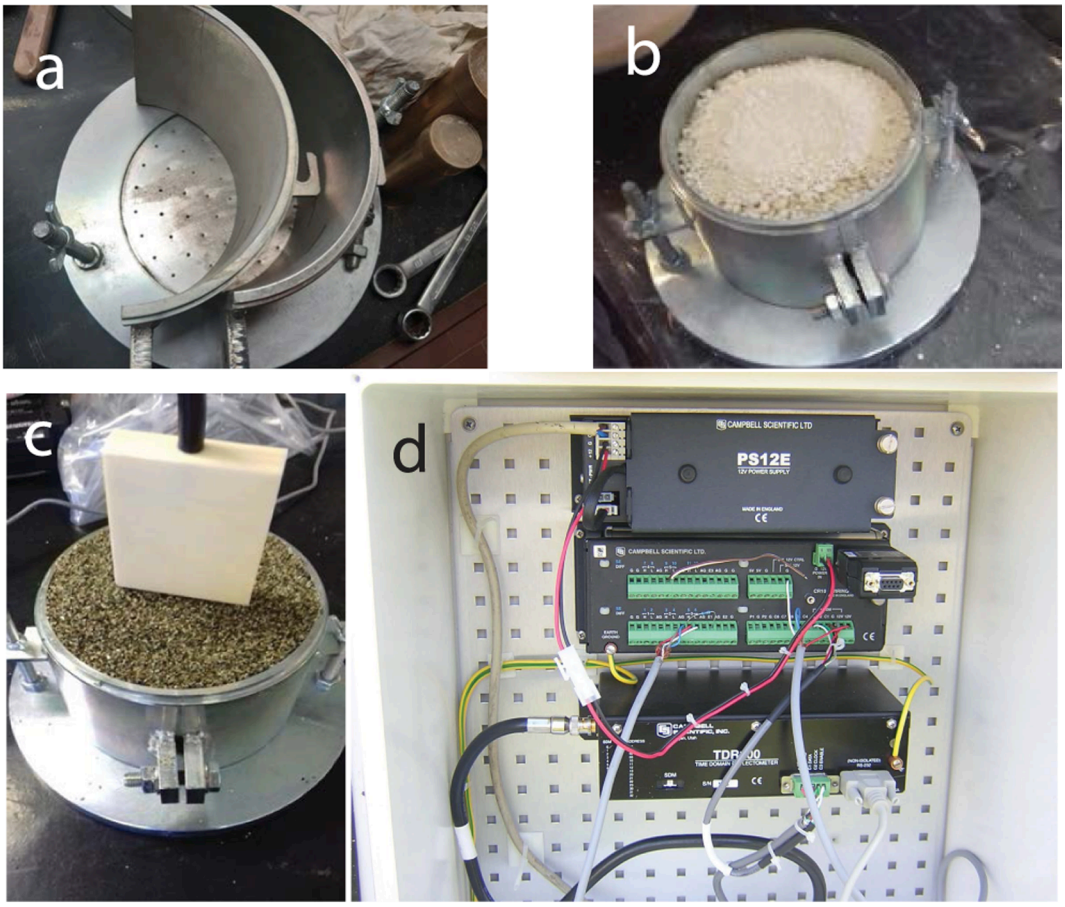

Fig. 3. Metal container (a), partially filled with kaolinite clay (b) and sand (c), during the preparation and TDR apparatus (d), using TDR 100 (from bottom to top in the box), CR10X Data logger and PS12E Rechargeable battery (Campbell Sci. Inc.).

The file `readDataFile` imports the experimental data. A specific file was written to open the data (instead of a generic open data file instruction), and incorporate a test over potential missing data or wrong data format. The interface allows for parameters modification, adjustment of water electric permittivity (ϵ_l) for temperature dependence and modification of solid phase electric permittivity (ϵ_s). The output includes visualization of travel times at point (1, 2 and 3) as shown in Fig. 1, visualization of bulk electric permittivity (ϵ_b), voltage attenuation and SWC output with the different equation presented above.

The file `functions` implements the functions to compute bulk electric permittivity, soil water content with the equations presented above and soil density with both the equation of Jung et al. (2013a) and Curioni et al. (2018).

The file `Marquardt` implements the Marquardt (1963) algorithm, while in the `travelTime` file is written the code to compute the travel time, including first and second derivative of the waveforms, tangent identification and others as described above. Since the Marquardt (1963) algorithm is dependent on the initial values of the parameters, the initial values were selected based on the values presented by Curioni et al. (2018) for soils having similar textural properties. Moreover, a convergence analysis showed that those initial parameters converged to the final fitted values without sitting in local minima.

Finally the file `plot` implements the functions to plot the graphs (Figs. 1, 2 and 4). The output data with the numerical values for SWC and SBD are printed in an output file and on the windows interface, as well as the fitted parameters. The structure of the software is modular and the program is written to be fully automatized such that the user can analyze hundreds or thousands of waveforms at a time, if necessary. The program is freeware available on GitHub.

4.1. Parametrization and statistical analysis

The model presented by Curioni et al. (2018) depends on the parameters as shown in Eq. 14. Since the method is fairly recent, there are not enough data in the literature to establish transfer relationships between basic soil properties (i.e. texture, mineralogy, organic matter content) and the parameters. Moreover, as discussed above the method does not allow for separating the effect of SBD and electrical conductivity on the attenuated voltage, therefore parametrization is quite sensitive on the soil conditions, and in particular on its ionic content.

For application of the method to our experimental data the parameters were calibrated. Many waveforms were collected for each sample and, after equilibrium was reached, waveform analysis did not provide significant differences in the computation of parameters.

An iterative method was written, to first collect the waveform, obtain the waveform parameters as described above and then adjust the parameters a, b and c. The parameters were iteratively changed to minimize the sum of square residuals between the measured SBD and the ones obtained from TDR, using the well known (Marquardt, 1963) least squares algorithm. While the Marquardt (1963) algorithm is implemented in many software such as R® or MatLab®, in this study the algorithm implemented in Python by Bittelli et al. (2015), was used.

The analysis of the waveform is performed only one time at the beginning of the analysis but the parameters in Eq. 14 are iteratively adjusted to obtain the best fit between independently and TDR-measured SBD.

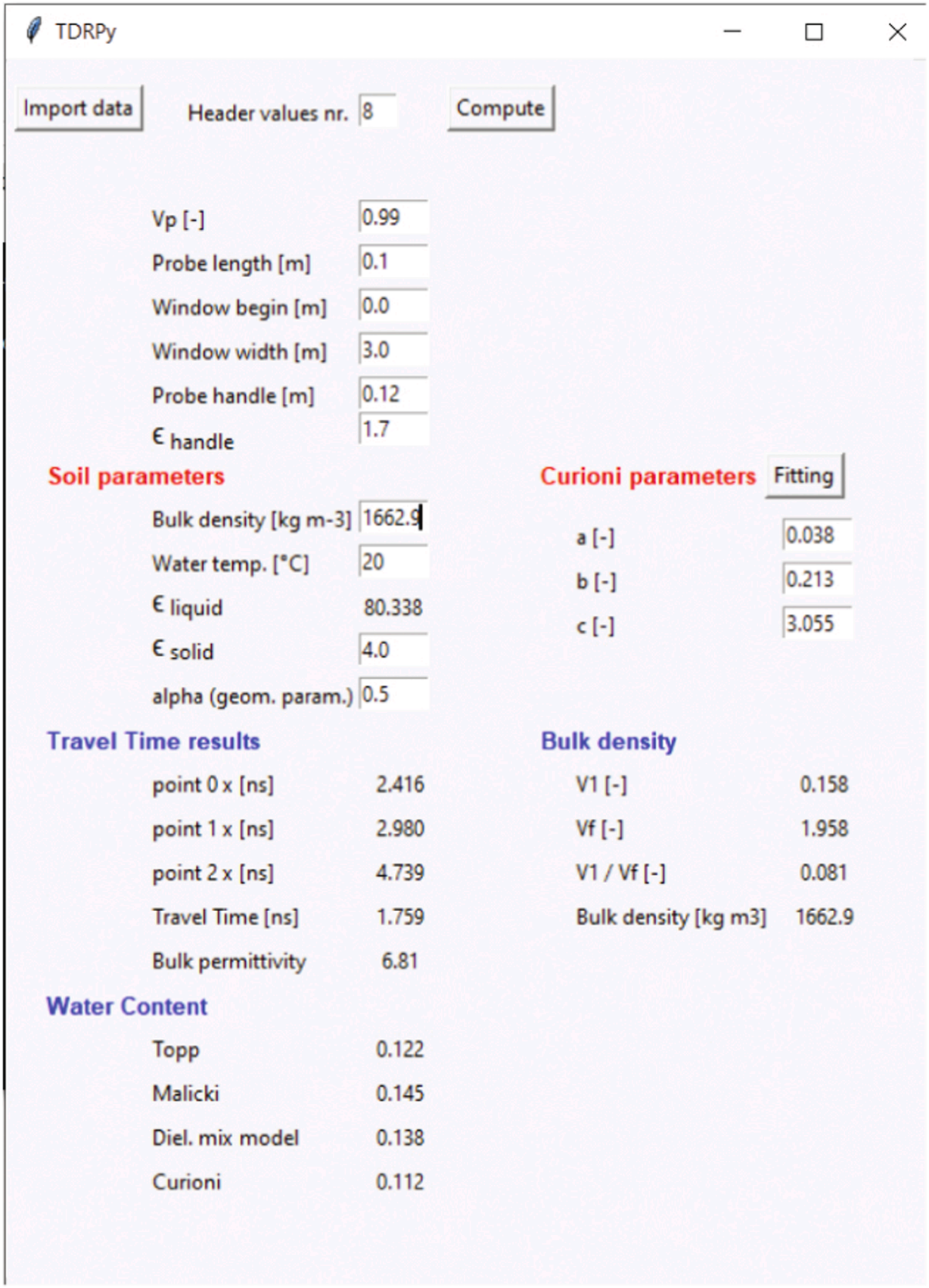

Fig. 4. Software interface (TDRPy).

5. Results and discussion

5.1. Soil bulk density

The accuracy of the proposed algorithm and method was tested by comparing the independent and the TDR-measured SBD. Table 1–3 list the independently measured SBD for sand, silty sand and kaolin respectively.

Fig. 5 shows a scatter plot, for all the samples combined but indicated by different colours, between independent and TDR-measured SBD. The parameters needed in Eq. 14 to obtain the TDR-measured SSD were obtained by the non-linear least squares procedure as described above and are listed in Table 4. The method provided good measurements of SBD for all the samples with Root Mean squared Error (RMSE) of 25, 16 and 40 kg m^{-3} for the sand, silty-sand and kaolinite samples respectively. The kaolinite sample provided a slightly less reliable estimation as also shown in Fig. 5.

The kaolinite sample was more difficult to wash for removal of ions in the solution, to remove the effect of EC. This could be a source of error, since the voltage attenuation is also affected by EC, as discussed above. Other source of potential error is the packing of the sample. However, measurement of saturated extract was low for kaolinite as well ($\leqslant$2 mS m^{-1}), assuring that the measurement was not significantly affected by EC.

In general the results of the analysis were satisfactory. Considering that the average densities were 1411 for sand, 1440 for silty-sand and 1209 kg m^{-3} for kaolinite and the RMSE was 25, 16 and 40 kg m^{-3}, the average error was 1.8, 1.1 and 3.3 % respectively. Overall, after an accurate calibration, the method was able to provide quite accurate measurements of SBD for three different type of materials.

5.2. Soil water content

Figs. 6 and 7 shows TDR-measured SWC against the independent gravimetric measurements, by using the four different equations described above, Topp et al. (1980), Malicki et al. (1996), Roth et al. (1990), Curioni et al. (2018).

As expected SWC estimation differed between the four equations and for the three samples. Table 5 shows the Pearson correlation coefficients (R) between the independently measured SWC and the TDR measured SWC, for the samples and the four equations. As shown in Table 1, the independent measurement of SWC for the sand sample ranged between about 0.06 to 0.07 (m^3 m^{-3}) (Table 1), with differences that are within the experimental error of the TDR 100 system which is ±2% (Robinson et al., 2003). Therefore the estimated data for sand are not discussed since they are not statistically significant, being the variation of the observed independent value within the error range.

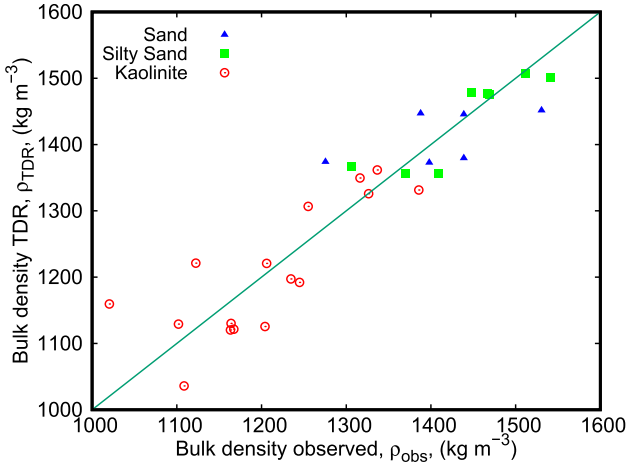

Fig. 5. Scatter plot of independently measured and TDR - measured SBD for all the samples. The different textures are indicated by symbols and colours. The black line is the 1:1 line.

Table 4
Soil-Specific coefficients obtained from the non-linear least squares optimization and root mean squared error.

	a	b	c	RMSE (kg m^{-3})
sand	0.041	0.291	3.64	25
silty sand	0.0	0.108	0.69	16
kaolinite	0.0	0.151	0.88	40

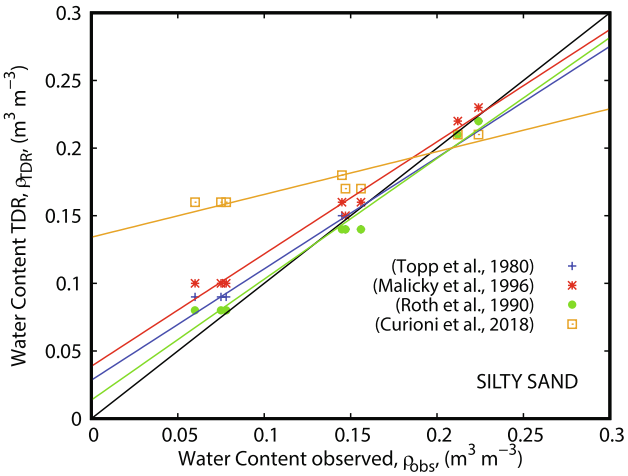

Fig. 6. Scatter plot of independently measured and TDR - measured SWC for the silty - sand samples. The four equations for SWC estimation are compared. Lines are guide for the eye. The black line is the 1:1 line.

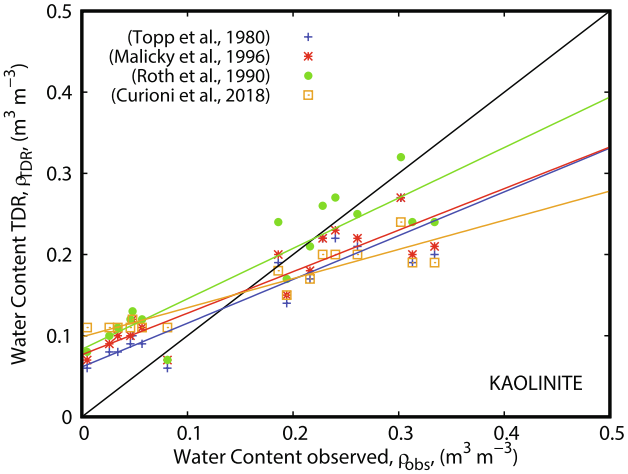

Fig. 7. Scatter plot of independently measured and TDR - measured SWC for the kaolinite samples. The four equations for SWC estimation are compared. Lines are guide for the eye. The black line is the 1:1 line.

Table 5
Correlation coefficients between the independently measured SWC and the TDR measured SWC, for the samples and the four equations.

	sand	silty-sand	kaolinite
Topp et al. (1980)	NA	0.9144	0.9830
Malicki et al. (1996)	NA	0.9139	0.9897
Roth et al. (1990)	NA	0.9380	0.9893
Curioni et al. (2018)	NA	0.9284	0.9256

Differently, for the silty-sand and the kaolinite samples, the estimation provided good results with high correlation coefficients as shown in Table 4, except for the Curioni et al. (2018) estimation of SWC, which displayed a lower correlation, in particular for the kaolinite sample (as also depicted in Fig. 7). Overall, the results for estimation of soil water content were also quite satisfactory, providing reliable estimation.

The reason for the lower correlation of the Curioni et al. (2018) model is due to its mathematical formulation for determining SWC. The model has a division term, with the electric permittivity directly multiplied by the density of water (which is treated as a constant at 20°) and divided by the SBD (Eq. 15). The formulation makes the estimation of SWC highly sensitive to SBD. While SBD is important in affecting water content, its effect is related to the relative contributions of the soil phases (solid, gas and liquid) as affected by porosity and not as a quotient term.

Indeed, as shown by Anbazhagan et al. (2020), a dielectric mixing model (Roth et al., 1990) provides the most accurate estimation of SWC, since it provides a weighted sum of the relative contributions of the individual electric permittivities. The solution of the dielectric mixing model (Eq. 20) shows that bulk electric permittivity ($\in_b$) is never directly divided or multiplied by SBD (ρ_d), while the solid phase electric permittivity ($\in_s$) is multiplied by the ratio (ρ_d/ρ_s) or the gas phase electric permittivity ($\in_g$) is multiplied by the porosity. Overall, this study confirms that the use of a dielectric mixing model is the best choice for estimation of SWC.

6. Conclusions

In this study: (a) a new algorithm was implemented into a software for simultaneous measurement of SWC and SBD using TDR, (b) the methodology developed to measure soil density from TDR was evaluated and tested against independently measured samples.

The software implements a method based on the first and second derivative of the waveform to obtain SWC and on the attenuation of the waveform to obtain SBD. The software allows for automated analysis of many TDR waveforms, including the possibility of using different equations for estimating SWC. Moreover, a non-linear least squares algorithm is incorporated into the software to obtain the unknown parameters of the Curioni et al. (2018) equation to obtain density.

The method was tested for three samples having different textural composition (sand, silty-sand and kaolinite), where independent measurements of SBD and SWC was performed. An optimization of the parameters was performed to asses the parameter variability and range, providing overall good results. The method was able to measure SBD with a small RMSE of 25, 16 and 40 kg m^{-3}, with an average error of 1.8, 1.1 and 3.3 % for sand, silty-sand and kaolinite respectively.

Measurements of SWC with TDR was confirmed to be an accurate method, with the dielectric mixing model of Roth et al. (1990) being the best formulation to derive SWC from electric permittivity, as also presented by Anbazhagan et al. (2020) when travel time theory was applied to ground penetrating radar. Since the estimation of SWC with the equation presented by Curioni et al. (2018) did not provide reliable estimates, it is suggested to revisit the equation proposed.

Overall, the presented methodology is a very promising method to measure soil density having many advantages with respect to the classic methods. There are still some key issues that must be addressed to make it a reliable method to use in practical applications and investigations:

1. Attenuation of the input TDR voltage depends on both electrical conductivity and density. Since in natural conditions soils display a given level of electrical conductivity, the method should be improved with the attempt to separate the effect of density from electrical conductivity. While in soils with low EC it may not determine a high error in the estimation of density, in other soils with higher EC the procedure may fail to provide accurate results. Methods have been used to separate the effect of σ_{DC} from density, such as discussed by Curioni et al. (2018). However, the proposed methods are simply based on parameters calibration. The uncertainty about contribution of electrical conductivity on the waveform attenuation is indeed contained in the parameter values. Clearly natural soils always contain ions. The method can be applied by identifying salinity (EC) limits of negligible influence where no EC correction is required.

   Overall, the natural variability of SBD in a region can undergo transformations that are less than the error the Curioni et al. (2018) formula proposes (Li et al., 2019), therefore making the method effective for spatial analysis of SBD.
2. At the moment there is no effective knowledge about the value of parameters. The number of soils and materials tested in the literature is very limited, such that no conclusions can be drawn about which parameters to choose for a given soil. The method, at the current state, requires calibration. It would be useful to obtain transfer equations (pedotransfer functions) allowing for correlation of the parameters to basic soil properties such as textural composition, mineralogy and organic matter content.

CRediT authorship contribution statement

Marco Bittelli: Conceptualization, Writing - original draft, Writing-review, Data Analysis, Software, Validation, Visualization, Funding acquisition, Methodology. **Fausto Tomei:** Data Analysis, Software, Validation, Visualization. **P. Anbazhagan:** Conceptualization, Funding acquisition, Project administration, Methodology. **Raghuveer Rao Pallapati:** Funding acquisition, Supervision, Writing - review & editing. **Pushkar Mahajan:** Data curation, Investigation. **Claudia Meisina:** Funding acquisition, Investigation, Methodology. **Massimiliano Bordoni:** Data curation, Investigation, Methodology. **Roberto Valentino:** Funding acquisition, Investigation, Methodology.

Declaration of Competing Interest

The authors declare that they have no known competing financial interests or personal relationships that could have appeared to influence the work reported in this paper.

Acknowledgements

This study was funded by: Project Scheme for Promotion of Academic and Research Collaboration (SPARC). A Government of India Initiative. Project Title: Prediction of Soil Hydro Agricultural Properties using Ground Penetrating Radar for Improving Agricultural Practice (Proposal ID: 375) and by the Department of Chemistry, Life Sciences and Environmental Sustainability, University of Parma, Italy. Project Leaders: Prof. Anbazhagan P. and Prof. Marco Bittelli. The software is available on the GitHub open source repository: https://github.com/ftomei/TDR-TravelTimeAnalysis or upon request to the first author, marco.bittelli@unibo.it. We thank the Editor and the Reviewers for the accurate and thorough reviews.

References

Al-Shammary, A.A.G., Kouzani, A.Z., Kaynak, A., Khoo, S.Y., Norton, M., Gates, W., 2018. Soil bulk density estimation methods: a review. Pedosphere 28 (4), 581–596.

Anbazhagan, P., Bittelli, M., Pallepati, R.R., Mahajan, P., 2020. Comparison of soil water content estimation equations using Ground Penetrating Radar. J. Hydrol. 588 (125039).

ASTM, 1963. Standard test method for particle-size analysis of soils. D422–63, West Conshohocken, PA.

ASTM, 2012. Standard test method for water content and density of soil in situ by time domain reflectometry (tdr). D6780M-12, West Conshohocken, PA.

ASTM, 2012. Standard test methods for laboratory compaction characteristics of soil using modified effort. D1557-12, West Conshohocken, PA.

ASTM, 2013. Standard test methods for density of soil and rock in place by the water replacement method in a test pit. D5030-D5030M-13a, West Conshohocken, PA, USA.
ASTM, 2015. Standard test method for density and unit weight of soil in place by the rubber balloon method. D2167-15, West Conshohocken, PA, USA.
ASTM, 2016. Standard test methods for density of soil and rock in place by the sand replacement method in a test pit. D4914M-16, West Conshohocken, PA, USA.
ASTM, 2017. Standard test method for density of soil in place by the drive-cylinder method. D2937-17, West Conshohocken, PA, USA.
Bittelli, M., Campbell, G.S., Tomei, F., 2015. Soil Physics with Python. Transport in the Soil-Plant-Atmosphere Continuum, first ed. Oxford University Press, Oxford, United Kingdom.
Burden, R., Faires, J., 1997. Numerical Analysis, 6th ed. Brooks and Cole, Washington.
Campbell Scientific Inc., 1986. CR10X datalogger (User Manual). Logan, UT, USA.
Campbell Scientific Inc., 2000. TDR 100 (User Manual). Logan, UT, USA.
Campbell Scientific Inc., 2015. CS610 3 Rod TDR Probe (User Manual). Logan, UT, USA.
Castiglione, P., Shouse, P., 2015. The effect of ohmic losses on TDR measurements of electrical conductivity. Soil Sci. Soc. Am. J. 67, 414–424.
Curioni, G., Chapman, D.N., Pring, L.J., Royal, A.C.D., Metje, N., 2018. Extending tdr capability for measuring soil density and water content for field condition monitoring. Geotech. J. 144 (2), 1–15.
Ferre', P., Knight, J., Rudolph, D., Kachanosky, R., 1998. The sample areas of conventional and alternative time domain reflectometry probes. Water Resour. Res. 34 (11), 2971–2979.
Giese, K., Tiemann, R., 1975. Determination of the complex permittivity from a thin sample time-domain reflectometry, improved analysis of the step response waveform. Adv. Molec. Relax. Processes 7, 45–59.
Grossman, R.B., Reinsch, T.G., 2002. Bulk density and linear extensibility. In: Dane, J.H., Topp, G.C. (Eds.), Methods of soil analysis, Part 1. Agron. Monogr. ASA, Madison, WI, pp. 128–152.
Heimovaara, T., de Water, E., 1993. A computer controlled tdr system for measuring water content and bulk electrical conductivity of soils. In: Laboratory of Physical Geography and Soil Science. University of Amsterdam.
Jung, S., Drnevich, V.P., Najm, M.R.A., 2013a. New methodology for density and water content by time domain reflectometry. Geotech. J. 139 (5), 659–670.
Jung, S., Drnevich, V.P., Najm, M.R.A., 2013b. Temperature corrections for time domain reflectometry parameters. Geotech. J. 139 (5), 671–683.
Li, S., Q, L.Q., C., W., B., L., X., G., Y., L., D., W., 2019. Spatial variability of soil bulk density and its controlling factors in an agricultural intensive area of chengdu plain, southwest china. J. Integr. Agric. 18(2), 290–300.
Malicki, M., Plagge, R., Roth, C., 1996. Improving the calibration of dielectric tdr soil moisture determination taking into account the solid soil. Eur. J. Soil Sci. 47, 357–366.
Marquardt, D.W., 1963. An algorithm for least-squares estimation of non-linear parameters. J. Soc. Ind. Appl. Math. 11, 431–441.
Olmi, R., Bittelli, M., 2015. Dielectric data analysis: recovering hidden relaxations by fourth-order derivative spectroscopy. IEEE Trans. Dielectr. Electr. Insul. 22 (6), 3334–3340.
Robinson, D.A., Jones, S.B., Wraith, J.M., Or, D., Friedman, S.P., 2003. A review of advances in dielectric and electrical conductivity measurement in soils using time domain reflectometry. Vadose Zone J. 2, 444–475.
Roth, K., Schulin, R., Fluhler, H., Attinger, W., 1990. Calibration of time domain reflectometry for water content measurement using a composite dielectric approach. Water Resour. Res. 26, 2267–2273.
Topp, G., Annan, J., Davis, A., 1980. Electromagnetic determination of soil water content: measurements in coaxial transmission lines. Water Resour. Res. 16, 574–582.